

Analysis of Soft-switching Converters for Switched Reluctance Motor Drives for Electric Vehicles

Tze Wood Ching

Department of Electromechanical Engineering, University of Macau, twching@umac.mo

Abstract

Two new soft-switching converters for switched reluctance motor drives are proposed and analyzed. The proposed zero-voltage-transition (ZVT) converter possesses the definite advantages that both main transistors and diodes can operate with zero-voltage switching (ZVS), as well as unity device voltage and current stresses. On the other hand, the proposed zero-current-transition (ZCT) converter offers the advantages that both the main and auxiliary switches operate with zero-current switching (ZCS), as well as minimum current and voltage stresses. Both converters have the merits of simple circuit topology, minimum component count and low cost.

Keywords

soft-switching converters, switched reluctance motor drives, electric vehicle propulsion

1. INTRODUCTION

The switched reluctance motor (SRM) drive is a kind of brushless motor drives, without any rotor conductors nor permanent magnets. The SRM operates on the force of magnetic attraction with the simplest configuration compared with the other types of brushless motors. The SRM drive has some definite advantages – simple and rugged construction, simple control, ability of extremely high speed operation, and hazard-free operation, these prominent advantages are very attractive for electric vehicle (EV) applications. It can also inherently operate with extremely long constant power range and highly favorable for vehicle traction application [Ehsani et al., 2007].

Within the past decades, the research and development on SRM drives have been focused on the motor topology design and optimization as well as the motor control strategies [Zhan et al., 1999; Chen et al., 2001; Chen et al., 2002; Chau and Chen, 2002; Chau and Chen, 2003]. Nevertheless, a number of converter topologies for SRM drives have also been proposed, such as the 1-switch per phase, 2-switch per phase, $(n + 1)$ -switch, $2(n + 1)$ -switch, C-dump and Oulton types [Miller, 1993]. However, all of these converter topologies employ the hard-switching technique which suffers from the drawbacks of high switching losses and severe electromagnetic interference (EMI). In recent years, a number of soft-switching techniques, providing either zero-voltage switching (ZVS) or zero-current switching (ZCS) condition, have been successfully developed for switched-mode power supplies [Ching, 2009] and has been extended to DC mo-

tor drives [Chau et al., 1999; Ching and Chau, 2001; Ching, 2005; Ching, 2006]. Also, a few studies on soft-switching converters for SRM drives have been reported [Murai et al., 1997; Cho et al., 1997; Rolim et al., 1999].

In this paper, two new soft-switching converters for SRM drives, namely the zero-voltage-transition (ZVT) converter, and zero-current-transition (ZCT) converter, are proposed and analysed. They possess some definite advantages over their hard-switching counterparts and other soft-switching converters. For the ZVT converter, it offers ZVS for all main switches and diodes, as well as unity device voltage and current stresses. For the ZCT converter, both the main and auxiliary switches can operate with ZCS, as well as minimum voltage and current stresses. Also, they both have simple circuit topology, hence minimum hardware count and low cost.

It should be noted that the ZVT topology, hence the ZVS condition, is highly desirable for power MOSFET based power conversion. It is due to the fact that the power MOSFET device generally suffers from severe capacitive voltage turn-on losses. On the other hand, the ZCT topology, hence the ZCS condition, is particularly favorable for IGBT based power conversion. The reason is due to the fact that the IGBT device generally suffers from severe inductive current turn-off losses.

2. SRM DRIVES

Figure 1 shows the circuit diagram of a conventional hard-switching converter for three-phase SRM drives. The upper chopping switch S_m serves all three phases while the lower commutating switches S_1 , S_2 and S_3 commutate the phases by selecting one phase at a time sequentially. As illustrated in Figure 2, the phase-1

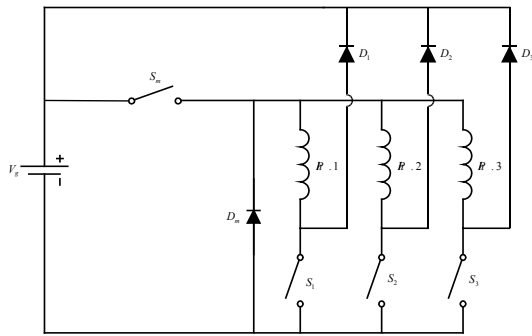


Fig. 1 Conventional converter for 3-phase SRM drives.

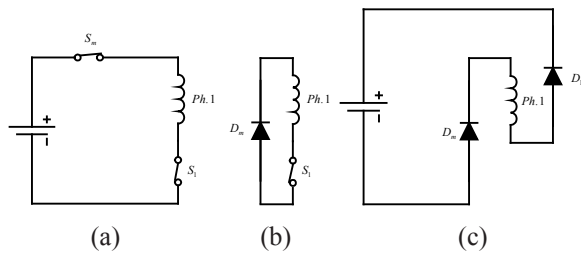


Fig. 2 Conduction modes for one phase

winding is excited by turning on S_1 , and the corresponding current can be controlled by switching S_m . Whenever S_m is turned off, the phase-1 current is free-wheeling via D_m . Whenever S_1 is turned off, the current is fed back to the source through D_m and D_1 . Thus the SRM drive can readily offer regenerative braking which is a key demand for EV application.

In general, SRM drives can operate in three different modes [Miller, 1993]:

- single-pulse mode,
- voltage-PWM chopping mode,
- current-regulated chopping mode

In the single-pulse mode, as shown in Figure 3, each

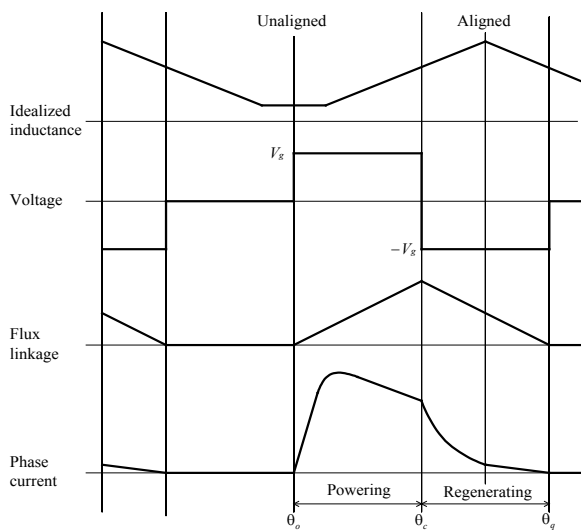


Fig. 3 Single-pulse waveforms

phase excites from zero during each stroke. The positive supply voltage is applied to the winding at the turn-on angle θ_o , and the current begins to rise as the rotor poles approach the stator poles of the next phase to be excited. Then, the negative supply voltage is applied at the commutation angle θ_c , and hence the flux linkage gradually drops to zero at the extinction angle θ_q .

The voltage-PWM chopping mode consists of two schemes, namely asynchronous chopping and synchronous chopping. The asynchronous chopping for phase-1 involves turning on S_1 for the full period between θ_o and θ_c , and switching S_m on and off at a high frequency with a fixed duty cycle during the same period. When S_m is on, the supply voltage is connected to the phase winding; otherwise, the winding is short-circuited through S_1 and D_m . On the other hand, in the voltage-PWM synchronous chopping mode, both S_m and S_1 synchronously switch together at a high frequency.

The current-regulated chopping mode employs a current regulator to turn on and off the power switches. Both synchronous and asynchronous chopping schemes are possible. A simple hysteresis controller can be used to maintain the current magnitude within the desired upper and lower limits. As the supply voltage is fixed, the switching frequency decreases as the incremental inductance of the phase winding increases.

3. PROPOSED ZVT CONVERTER

Figure 4 shows the schematic diagram of the proposed ZVT converter for SRM drives. To achieve ZVT operation, there are two resonant tanks. First, a resonant inductor L_a , a resonant capacitor C_a , an auxiliary switch S_a and an auxiliary diode D_a are added to allow for soft-switching S_m . Second, a resonant inductor L_b , three resonant capacitors C_{b1} , C_{b2} , C_{b3} , an auxiliary switch S_b and four diodes D_b , D_{b1} , D_{b2} , D_{b3} are added to allow for soft-switching S_1 , S_2 and S_3 .

A simplified per-phase circuit diagram is shown in

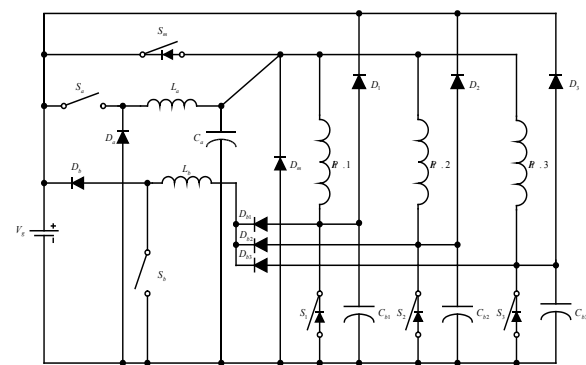


Fig. 4 Proposed ZVT converter

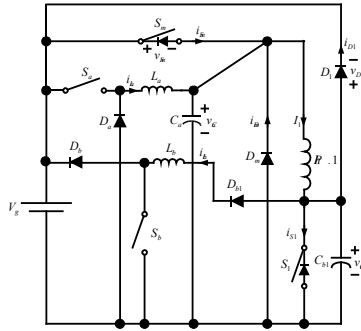


Fig. 5 Simplified per-phase circuit diagram

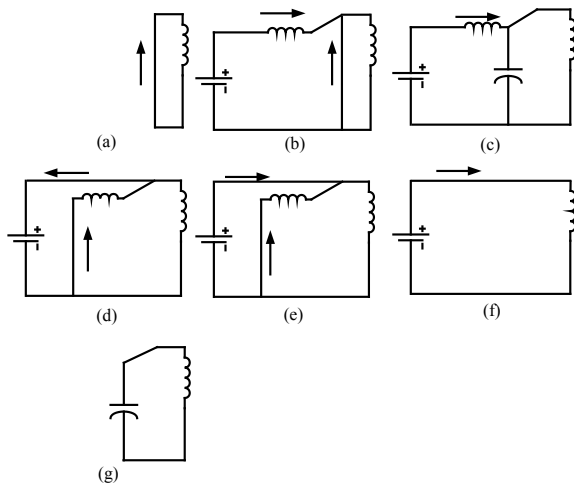


Fig. 6 Equivalent circuit of ZVT converter (powering)

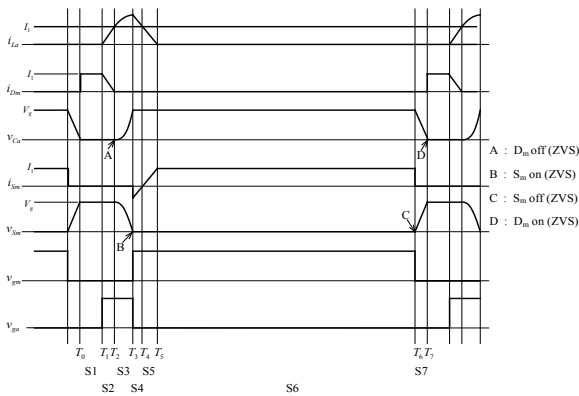


Fig. 7 Key waveforms of ZVT converter (powering)

Figure 5. The phase winding can be considered to be simultaneously fed by a buck converter (involving S_m and D_m) and a boost converter (involving S_1 and D_1). The corresponding equivalent circuits and operating waveforms are shown in Figures 6 to 9. It can be found that both equivalent circuits involve seven operating stages (S1 to S7) within one switching cycle.

3.1 Powering operation of ZVT converter (see Figures 6 and 7)

(a) Stage 1 [T_0 - T_1]: The phase winding is freewheel-

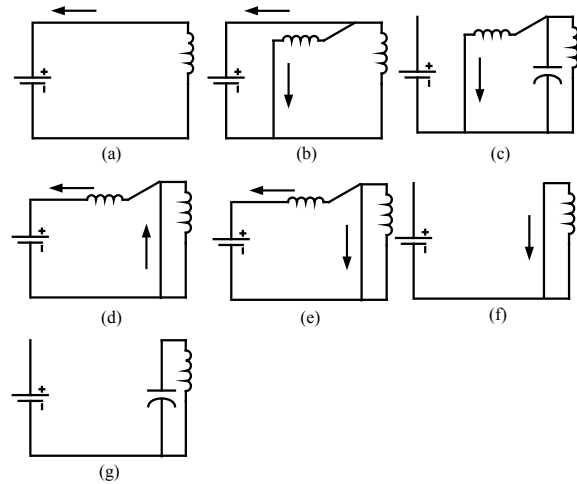


Fig. 8 Equivalent circuit of ZVT converter (regenerating)

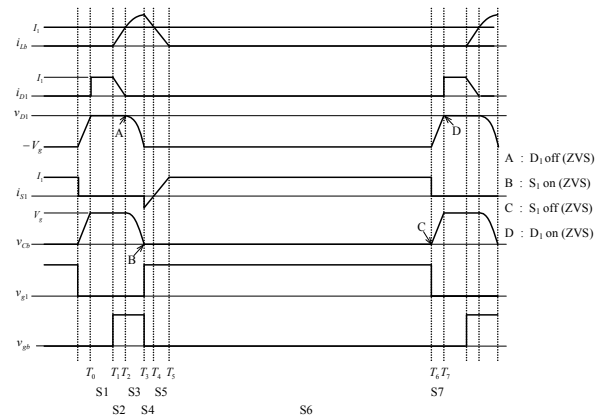


Fig. 9 Key waveforms of ZVT converter (regenerating)

- ing with I_1 via D_m .
- (b) Stage 2 [T_1 - T_2]: S_a is turned on. Then i_{La} increases linearly according to the slope of V_g/L_a . This stage finishes at T_2 when i_{La} equals I_1 .
- (c) Stage 3 [T_2 - T_3]: When $i_{La} = I_1$, D_m is turned off with ZVS, and L_a and C_a start resonating. This stage ends at T_3 when v_{Ca} equals V_g .
- (d) Stage 4 [T_3 - T_4]: When v_{Ca} reaches V_g , S_m is turned on with ZVS. S_a is turned off to recover the stored energy in L_a to the source. Then i_{La} flows through D_a and decreases linearly with a slope of V_g/L_a . At T_4 , i_{La} decreases to I_1 and i_{Sm} crosses zero from negative to positive.
- (e) Stage 5 [T_4 - T_5]: i_{La} keeps decreasing while i_{Sm} increasing until i_{La} reaches zero at T_5 and D_a becomes off.
- (f) Stage 6 [T_5 - T_6]: It is a powering stage. V_g is directly connected to the phase winding via S_m and S_1 .
- (g) Stage 7 [T_6 - T_7]: I_1 discharges C_a linearly with a slope of I_1/C_a until v_{Ca} equals zero at T_7 , and even-

tually D_m becomes turn-on with ZVS.

3.2 Regenerating operation of ZVT converter (see Figures 8 and 9)

- (a) Stage 1 $[T_0-T_1]$: D_1 is conducting, and it is a regenerating stage.
- (b) Stage 2 $[T_1-T_2]$: S_b is turned on. i_{L_b} increases with the slope of V_g/L_b . This stage finishes at T_2 when i_{L_b} equals I_1 .
- (c) Stage 3 $[T_2-T_3]$: When i_{L_b} reaches I_1 at T_2 , D_1 becomes turn-off with ZVS, and L_b and C_b start resonating. At T_3 , v_{Cb} decreases to zero.
- (d) Stage 4 $[T_3-T_4]$: When v_{Cb} reaches zero, S_1 is turned on with ZVS. S_b is turned off to recover the stored energy in L_b to the source. Then i_{L_b} flows through D_b and D_{b1} , and decreases linearly. At T_4 , i_{L_b} decreases to I_1 and i_{S1} crossed zero from negative to positive.
- (e) Stage 5 $[T_4-T_5]$: i_{L_b} keeps decreasing and i_{S1} increasing until i_{L_b} reaches zero at T_5 . D_b and D_{b1} become off.
- (f) Stage 6 $[T_5-T_6]$: The phase winding is freewheeling with I_1 .
- (g) Stage 7 $[T_6-T_7]$: I_1 charges C_b linearly with a slope of I_1/C_b until v_{Cb} equals V_g at T_7 , and eventually D_1 becomes turn-on with ZVS.

4. PROPOSED ZCT CONVERTER

As shown in Figure 10, two resonant tanks are added to form the proposed ZCT converter for SRM drives.

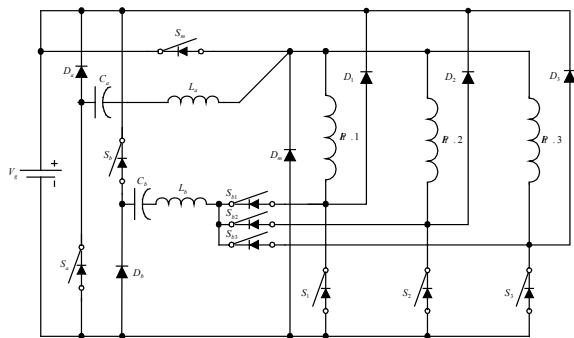


Fig. 10 Proposed ZCT converter

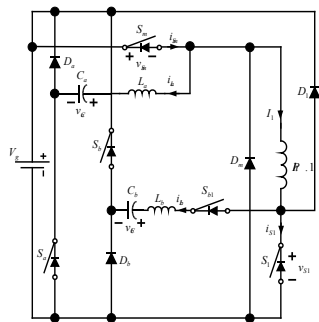


Fig. 11 Simplified per-phase circuit diagram

A resonant inductor L_a , a resonant capacitor C_a , an auxiliary switch S_a and an auxiliary diode D_a are added to allow for soft-switching S_m . A resonant inductor L_b , a resonant capacitors C_b , an auxiliary diode D_b , and four auxiliary switches S_b , S_{b1} , S_{b2} , and S_{b3} are added to allow for soft-switching S_1 , S_2 , and S_3 . A simplified per-phase circuit diagram is shown in Figure 11.

Similar to the ZVT converter, the phase winding can also be considered to be simultaneously fed by a buck converter (involving S_m and D_m) and a boost converter (involving S_1 and D_1). The corresponding equivalent circuits and operating waveforms are shown in Figures 12 to 15. It can be found that both equivalent

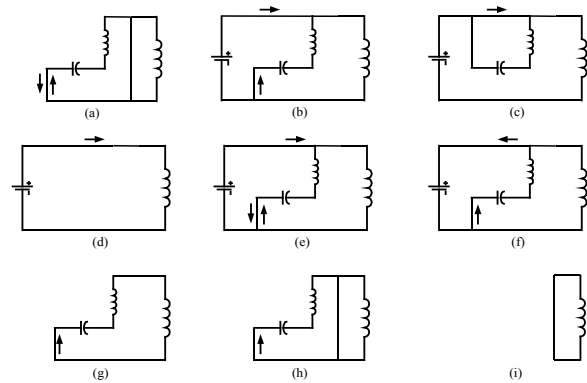


Fig. 12 Equivalent circuit of ZCT converter (powering)

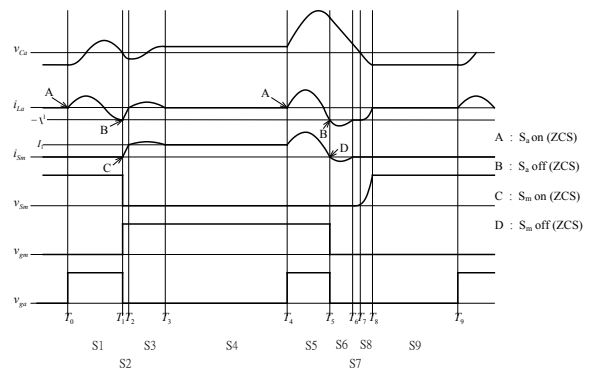


Fig. 13 Key waveforms of ZCT converter (powering)

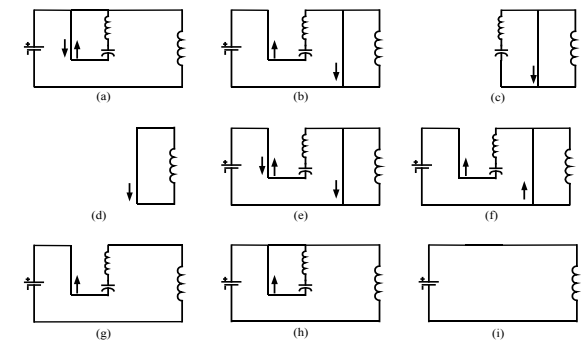


Fig. 14 Equivalent circuit of ZCT converter (regenerating)

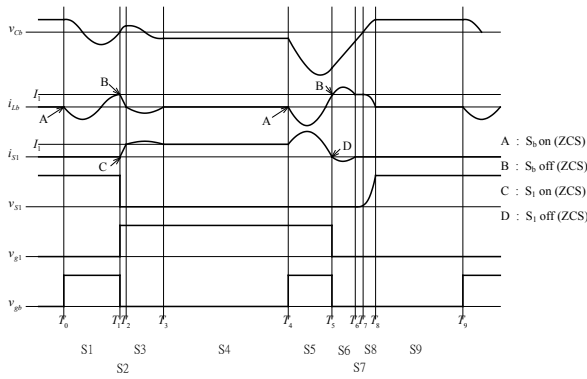


Fig. 15 Key waveforms of ZCT converter (regenerating)

circuits involve nine operating stages (S_1 to S_9) within one switching cycle.

4.1 Powering operation of ZCT converter (see Figures 12 and 13)

- (a) Stage 1 [T_0 - T_1]: S_a is turned on with ZCS at T_0 . L_a and C_a start resonating. i_{La} increases from zero to peak, then decreases towards zero, and then changes its direction. This stage finishes at T_1 when i_{La} reaches $-I_1$ so that D_m becomes off.
- (b) Stage 2 [T_1 - T_2]: S_a is turned off while S_m is turned on with ZCS at T_1 . The current of D_m is directed to the auxiliary circuit. i_{La} increases rapidly towards zero. This stage finishes at T_2 when i_{La} reaches zero.
- (c) Stage 3 [T_2 - T_3]: Since i_{La} becomes positive at T_2 . The antiparallel diode of S_a is off while D_a becomes on. L_a and C_a continue resonating. When i_{La} returns to zero at T_3 , D_a turns off naturally.
- (d) Stage 4 [T_3 - T_4]: It is a powering stage. V_g is directly connected to the phase winding via S_m and S_1 .
- (e) Stage 5 [T_4 - T_5]: S_a is turned on with ZCS. L_a and C_a start resonating. i_{La} increases from zero to peak, then decreases towards zero, and then changes its direction. When it reaches $-I_1$ at T_5 , the antiparallel diode of S_a becomes on.
- (f) Stage 6 [T_5 - T_6]: S_m is turned off with ZCS at T_5 . As i_{La} keeps decreasing, its negative surplus flows through the antiparallel diode of S_m . At T_6 , i_{La} swings back to $-I_1$ and the antiparallel diode of S_m stops conducting.
- (g) Stage 7 [T_6 - T_7]: i_{La} keeps at $-I_1$ and v_{Ca} is linearly discharged towards zero. This stage ends at T_7 when v_{Ca} reaches zero.
- (h) Stage 8 [T_7 - T_8]: At T_7 , D_m starts to conduct. i_{La} and v_{Ca} resonate again and i_{La} reaches zero at T_8 .
- (i) Stage 9 [T_8 - T_9]: The phase winding is freewheeling with I_1 via D_m .

4.2 Regenerating operation of ZCT converter (see Figures 14 and 15)

- (a) Stage 1 [T_0 - T_1]: S_b and S_{b1} are turned on with ZCS. L_b and C_b start resonating. When i_{Lb} decreases from zero to negative peak, then increases towards zero, and then changes its direction. i_{Lb} reaches I_1 at T_1 and D_1 becomes off.
- (b) Stage 2 [T_1 - T_2]: Both S_b is turned off with ZCS and S_1 is turned on with ZCS at T_1 . i_{Lb} decreases towards zero. This stage finishes at T_2 when i_{Lb} reaches zero.
- (c) Stage 3 [T_2 - T_3]: Since i_{Lb} becomes negative at T_2 . The antiparallel diode of S_b is off while D_b becomes on. L_b and C_b continue resonating. i_{Lb} returns to zero while both S_{b1} is turned off with ZCS and D_b is turned off naturally at T_3 .
- (d) Stage 4 [T_3 - T_4]: The phase winding is freewheeling with I_1 via S_1 .
- (e) Stage 5 [T_4 - T_5]: S_b and S_{b1} are turned on with ZCS. L_b and C_b start resonating. i_{Lb} decreases from zero to negative peak, then increases towards zero, and then changes its direction. When it reaches I_1 at T_5 , the antiparallel diode of S_1 becomes on.
- (f) Stage 6 [T_5 - T_6]: S_1 is turned off with ZCS at T_5 . As i_{Lb} keeps increasing, its surplus flows through the antiparallel diode of S_1 . At T_6 , i_{Lb} swings back to I_1 and the antiparallel diode of S_1 stops conducting.
- (g) Stage 7 [T_6 - T_7]: i_{Lb} keeps at I_1 and v_{Cb} is linearly discharged towards zero. This stage ends at T_7 when v_{Cb} reaches zero.
- (h) Stage 8 [T_7 - T_8]: At T_7 , D_1 starts to conduct. i_{Lb} and v_{Cb} resonate again and i_{Lb} reaches zero at T_8 .
- (i) Stage 9 [T_8 - T_9]: It is a regenerating stage via D_1 .

5. SIMULATION AND VERIFICATION

5.1 Results of ZVT converter

Different modes of operation of the proposed ZVT converter for SRM drives are PSpice-simulated. Figure 16 shows the simulated waveforms of the proposed converter operating in the single-pulse mode. The supply voltage turns on at the turn-on angle θ_{os} and then turns off at the commutation angle θ_c . Operating waveforms of the voltage-PWM asynchronous chopping mode is shown in Figure 17. S_1 is turned on for the full period between θ_{os} and θ_c , and S_m is turned on and off at a high frequency with a fixed duty cycle during the same period. Figure 18 shows the operating waveforms of the ZVT converter operating in the voltage-PWM synchronous chopping mode. Both S_m and S_1 simultaneously switch together at a high frequency. To obtain the simulation waveforms in Figure 19, a hysteresis current controller is used to maintain the current magnitude within the upper and lower limits of the proposed converter, so-called the current-

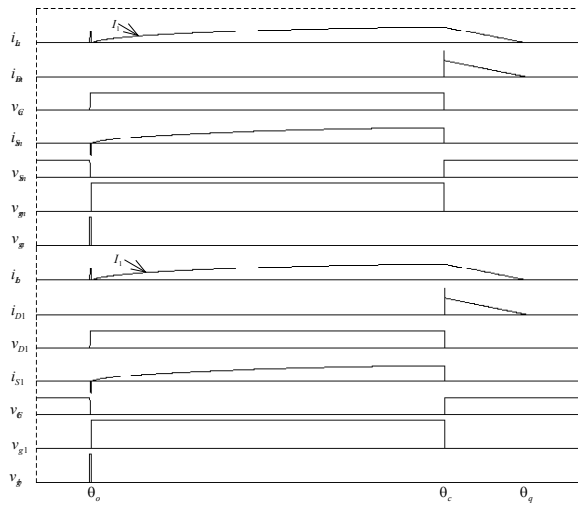


Fig. 16 PSpice-simulated waveforms of ZVT converter at single-pulse mode

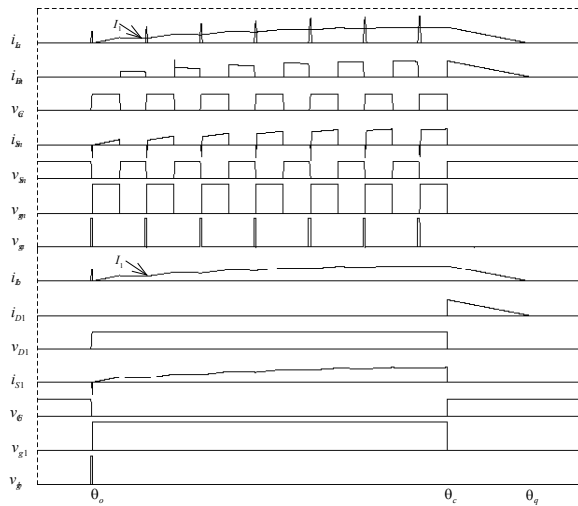


Fig. 17 PSpice-simulated waveforms of ZVT converter at voltage-PWM asynchronous chopping mode

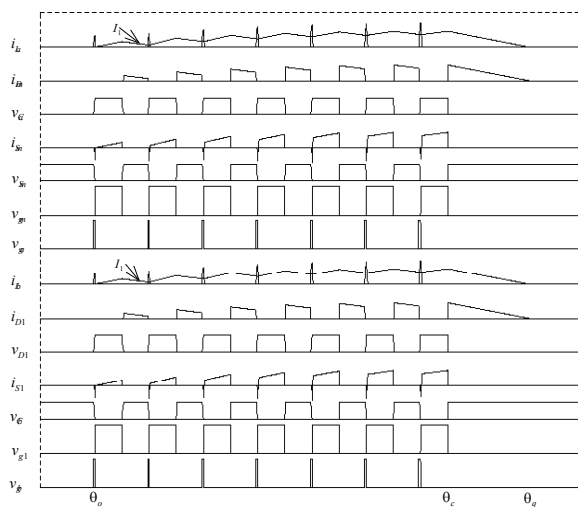


Fig. 18 PSpice-simulated waveforms of ZVT converter at voltage-PWM synchronous chopping mode

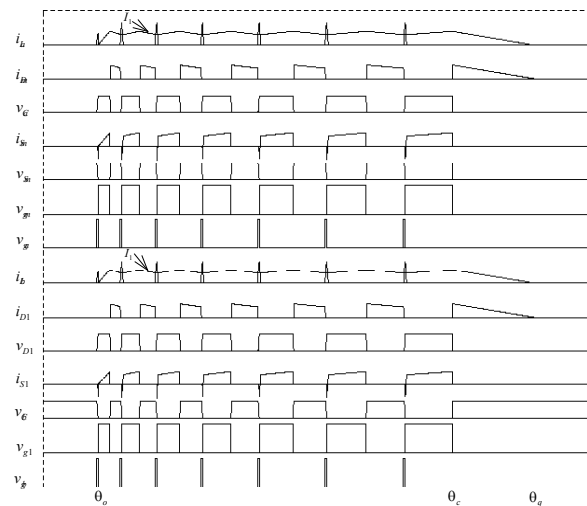


Fig. 19 PSpice-simulated waveforms of ZVT converter at current-regulated synchronous chopping mode

regulated synchronous chopping mode. The simulation results agree with those theoretical waveforms. The main switches and diodes of the converter (S_m , D_m and S_1 , D_1) can always maintain ZVS operation. As shown in Figure 20, the main switches (v_{Sm} and v_{S1}) and diodes (v_{Dm} and v_{D1}) operate with ZVS, and they are subjected to the same voltage and current stresses as those in the PWM counterpart. Nevertheless, the two auxiliary switches still suffer from hard-switching operation. Since the power involved in these auxiliary switches is only a fraction of the total power handled by the main switches, the hard-switching turn-off losses of the auxiliary circuitry can be outweighed by the reduction of switching losses in the main circuitry.

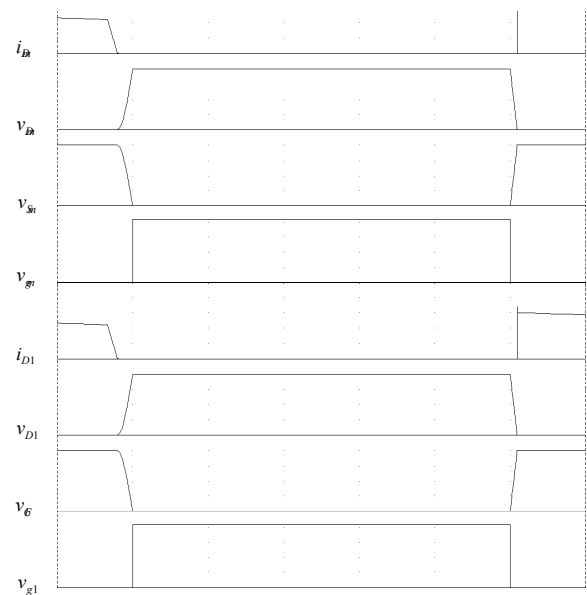


Fig. 20 Zero-voltage turn-on/turn-off condition

5.2 Results of ZCT converter

Different modes of operation of the proposed ZCT converter for SRM drives are also PSpice-simulated. Figure 21 shows the simulated waveforms of the proposed converter operating in the single-pulse mode. The supply voltage turns on at the turn-on angle θ_o , and then turns off at the commutation angle θ_c . Operating waveforms of the voltage-PWM asynchronous chopping mode is shown in Figure 22. S_1 is turned on for the full period between θ_o and θ_c , and S_m is turned on and off at a high frequency with a fixed duty cycle during the same period. Figure 23 shows the operating waveforms of the ZCT converter operating in voltage-PWM synchronous chopping mode. Both S_m and S_1 are switched together at a high frequency. Figure 24 shows the waveforms in the current-regulated synchronous chopping mode, where a hysteresis controller is used to maintain the current magnitude within

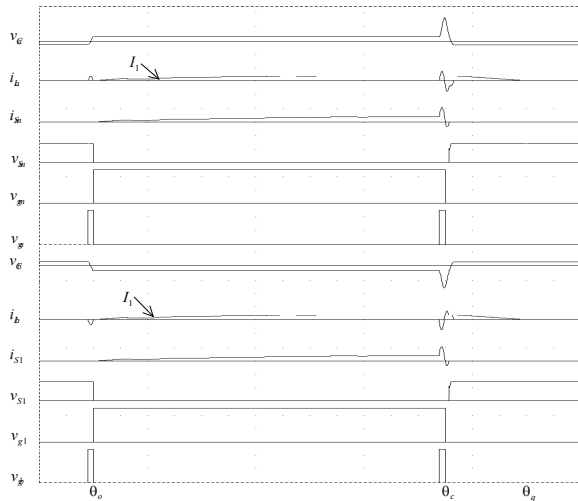


Fig. 21 PSpice-simulated waveforms of ZCT converter at single-pulse mode

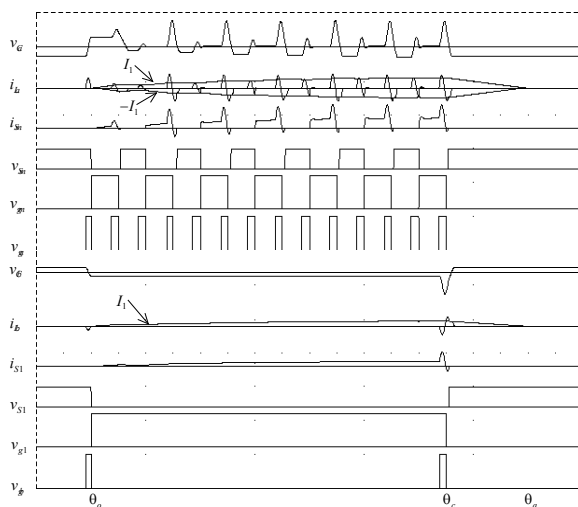


Fig. 22 PSpice-simulated waveforms of ZCT converter at voltage-PWM asynchronous chopping

the upper and lower limits. As expected, all these simulation results agree well with these theoretical waveforms. As shown in Figure 25, both the main and auxiliary switches of the proposed ZCT converter (S_m , S_a , S_1 and S_b) can always operate with ZCS.

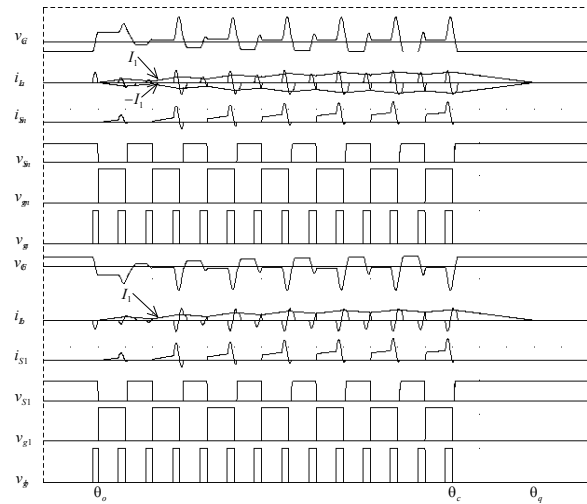


Fig. 23 PSpice-simulated waveforms of ZCT converter at voltage-PWM synchronous chopping mode

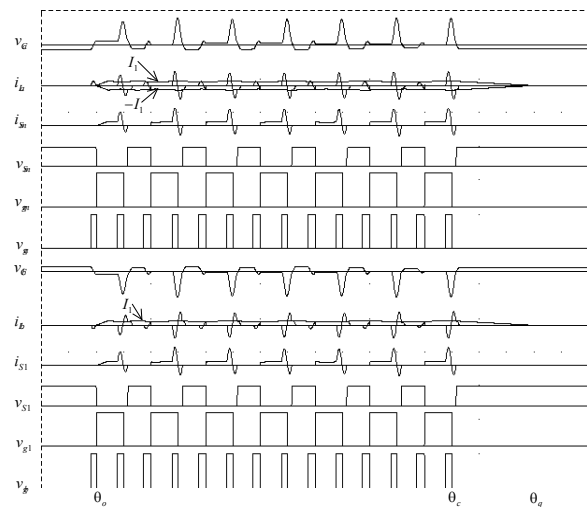


Fig. 24 PSpice-simulated waveforms of ZCT converter at current-regulated synchronous chopping mode

6. CONCLUSION

Two new soft-switching converters for SRM drives has been presented. The ZVT converter possesses the definite advantages that all main switches and diodes can achieve ZVS while the corresponding device voltage and current stresses are kept at unity. It is a very desirable feature for high frequency switching power conversion where MOSFETs are used because of their severe capacitive turn-on losses. The new ZCT converter possesses the advantages that both the main and auxiliary switches can always maintain ZCS with minimum current and voltage stresses. Both the pro-

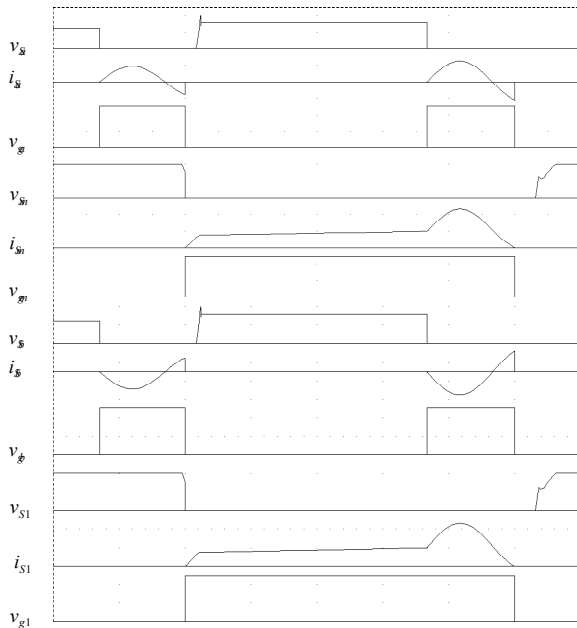


Fig. 25 Zero-current turn-on/turn-off condition

posed soft-switching converters utilize simple circuit topology, hence minimum hardware count and low cost, leading to achieve high power density and high efficiency.

References

Chau, K. T., T. W. Ching, and C. C. Chan, A new two-quadrant zero-voltage transition converter for DC motor drives, *International Journal of Electronics*, Vol. 86, No. 2, 217-231, 1999.

Chau, K. T., and J. H. Chen, Analysis of chaotic behavior in switched reluctance motors using current hysteresis regulation, *Electric Power Components and Systems*, Vol. 30, 607-624, 2002.

Chau, K. T., and J. H. Chen, Modeling, analysis and experimentation of chaos in a switched reluctance drive system, *IEEE Transactions on Circuits and Systems-I*, Vol. 50, No. 5, 712-716, 2003.

Chen, J. H., K. T. Chau, and Q. Jiang, Analysis of chaotic behavior in switched reluctance motors using voltage PWM regulation, *Electric Power Components and Systems*, Vol. 29, 211-227, 2001.

Chen, J. H., K. T. Chau, C. C. Chan, and Q. Jiang, Subharmonics and chaos in switched reluctance motor drives, *IEEE Transactions on Energy Conversion*, Vol. 17, No. 1, 73-78, 2002.

Ching, T. W., and K. T. Chau, A new two-quadrant zero-current transition converter for DC motor drives, *International Journal of Electronics*, Vol. 88, No. 6, 719-735, 2001.

Ching, T. W., Four-quadrant zero-voltage-transition converter-fed DC motor drives for electric propulsion, *Journal of Asian Electric Vehicles*, Vol. 3, No.

1, 651-656, 2005.

Ching, T. W., Four-quadrant zero-current-transition converter-fed DC motor drives for electric propulsion, *Journal of Asian Electric Vehicles*, Vol. 4, No. 2, 911-918, 2006.

Ching, T. W., Review of soft-switching technologies for high-frequency switched-mode power conversion, *International Journal of Electrical Engineering Education*, Vol. 46, No. 1, 121-136, 2009.

Cho, J. G., W. H. Kim, G. H. Rim, and, K. Y. Cho, Novel zero transition PWM converter for switched reluctance motor drives, *Proceedings of IEEE Power Electronics Specialists Conference*, 887-891, 1997.

Ehsani, M., Y. Gao, and J. M. Miller, Hybrid electric vehicles: Architecture and motor drives, *Proceedings of the IEEE*, Vol. 95, No. 4, 719-728, 2007.

Miller, T. J. E., *Switched reluctance motors and their control*, Oxford Science Publications, 1993.

Murai, Y., J. Cheng, and M. Yoshida, A soft-switched reluctance motor drives circuit with improved performances, *Proceedings of IEEE Power Electronics Specialists Conference*, 881-886, 1997.

Rolim, L. G. B., W. I. Suemitsu, E. H. Watanabe, and R. Hanitsch, Development of an improved switched reluctance motor drive using a soft-switching converter, *IEE Proceedings-Electric Power Applications*, Vol. 146, No. 5, 488-494, 1999.

Zhan, Y. J., C. C. Chan, and K. T. Chau, A novel sliding-mode observer for indirect position sensing of switched reluctance motor drives, *IEEE Transactions on Industrial Electronics*, Vol. 46, No. 2, 390-397, 1999.

(Received December 22, 2008; accepted February 2, 2009)